



ELSEVIER

Contents lists available at ScienceDirect

Journal of Solid State Chemistry

journal homepage: www.elsevier.com/locate/jssc

The $RELi_xSn_2$ ($RE=La-Nd, Sm, \text{ and } Gd; 0 \leq x < 1$) series revisited. Synthesis, crystal chemistry, and magnetic susceptibilities

Julien P.A. Makongo^a, Nian-Tzu Suen^a, Shengping Guo^a, Shanta Saha^b, Richard Greene^b, Johnpierre Paglione^b, Svilen Bobev^{a,*}

^a Department of Chemistry and Biochemistry, University of Delaware, Newark, DE 19716, USA

^b Department of Physics, University of Maryland, College Park, MD 20742, USA

ARTICLE INFO

Article history:

Received 9 October 2013

Received in revised form

3 December 2013

Accepted 10 December 2013

Available online 21 December 2013

Keywords:

Crystal structure

Single-crystal X-ray diffraction

Electronic structure calculations

Lanthanides

Lithium

Tin

ABSTRACT

This study is concerned with the ternary compounds $RELi_xSn_2$ ($RE=La-Nd, Sm, \text{ and } Gd; 0 \leq x < 1$), which have been previously thought to be the stoichiometric $RELiSn_2$ phases. These materials crystallize with the base-centered orthorhombic space group $Cmcm$ (No. 63), and can be formally assigned with the $CeNiSi_2$ structure type (Pearson symbol $oC16$). Our systematic single-crystal X-ray diffraction studies revealed substantial Li-deficiencies in all cases, with $SmSn_2$ (space group $Cmmm$, $ZrGa_2$ structure type, Pearson symbol $oC12$) and $GdSn_2$ (space group $Cmcm$, $ZrSi_2$ structure type, Pearson symbol $oC12$) being completely lithium-free. The structure refinements also uncovered positional disorder on the Sn site neighboring the vacancies. The Sn-disorder and the Li-deficiency correlate, and vary monotonically with the decreased size of the rare-earth atoms in the order $RE=La-Nd$. The $SmSn_2$ and $GdSn_2$ structures are devoid of any disorder. Temperature-dependent studies of the magnetic response of the title compounds are also presented and discussed.

© 2013 Elsevier Inc. All rights reserved.

1. Introduction

In recent years, our research group has investigated in depth the ternary $RE-Li-Ge$ systems, and we have already reported on the crystal chemistry and physical properties of a large variety of ternary compounds—these include $RELiGe_2$ ($RE=La-Nd, Sm, \text{ and } Eu$) [1], $RE_2Li_2Ge_3$, $RE_3Li_4Ge_4$, $RE_7Li_8Ge_{10}$, and $RE_{11}Li_{12}Ge_{16}$ ($RE=La-Nd, Sm$), with the last four being members of the extended homologous series $[REGe_2]_n[RELi_2Ge]_m$ [2,3]. Over the course of the structural work, we stipulated that the “electron shortages” in some of these structures are overcome via admixture of Li and Ge (on the Li site). Thus, to unequivocally establish such conjecture, our attention was focused on the possible existence of stannide analogs of $RE_3Li_{4-x}Ge_{4+x}$ [2]. As a result we successfully synthesized and characterized $Ce_3Li_{3.69}Sn_{4.31(1)}$, isotypic with $Ce_3Li_{3.95}Ge_{4.05(1)}$, where the magnitude of the Li–Sn substitution was much clearer [2]. Accidentally, the Ce–Li–Sn reaction also afforded $CeLi_{0.63(1)}Sn_2$, a phase with unit cell parameters very close to those of the known compound $CeLiSn_2$ ($CeNiSi_2$ structure type) [4,5], yet Li-deficient. With this respect, we note that Pavlyuk et al. [4], who explored initially the ternary $RE-Li-Sn$ systems, identified the $RELiSn_2$ ($RE=La-Nd, Sm, Gd-Tm, Lu$) compounds from powder

X-ray diffraction data (structure refined only for $CeLiSn_2$) [4]. The authors noted in their communication the existence of many non-stoichiometric RET_xX_2 ($0 < x < 1$; T stands for late transition metal, and $X=Si, Ge, \text{ and } Sn$) [5], and alluded to the possibility for a wide homogeneity range in $RELi_xSn_2$ ternaries. Nonetheless, based on the variation of the unit cell parameters on going from La to Lu, and comparing the unit cell volumes with those of the corresponding binary phases $RESn_2$ ($ZrSi_2$ structure type) [6–8], presumed them all to be stoichiometric and isostructural with the $CeNiSi_2$ structure [5,9].

With this study, we carefully revise the crystal structures of the $RELi_xSn_2$ ($RE=La-Nd, 0 \leq x < 1$) compounds using single-crystal X-ray diffraction data. Interestingly, the structural data uncovered that the phase width, i.e., the partial occupation of the Li position is accompanied by a positional disorder on the next-nearest Sn neighbor. Consequently, the Sn1 positions are split into two distinct Sn1A and Sn1B sites, leading to intricate disorder. The Li off-stoichiometry and the concomitant Sn disorder mirror the lanthanide contraction, and on the basis of this work, we speculate that the crystal structures of $RELi_xSn_2$ series has a “break-point” for $RE=Sm$, i.e., the Li uptake becomes diminutive. Thus, the major product of the Sm–Li–Sn reaction is the binary $SmSn_2$ phase, which is isotypic with $NdSn_2$ ($ZrGa_2$ structure type, space group $Cmmm$, Pearson symbol $oC12$) [5,10]. Similarly, the major product of the Gd–Li–Sn reaction is the binary $GdSn_2$ phase ($ZrSi_2$ structure type, space group $Cmcm$, Pearson symbol $oC12$) [5,11]. We present

* Corresponding author. Tel.: +1 302 831 8720; fax: +1 302 831 6335.
E-mail address: bobev@udel.edu (S. Bobev).

and compare all structures and review the magnetic susceptibilities of these compounds, particularly in comparison with the previous work [4,7,8]. The electronic band structures, calculated with the aid of the TB-LMTO method [12] are also discussed.

2. Experimental

2.1. Synthesis

All starting materials and products of the present investigation were handled and stored inside an Argon-filled glove box atmosphere due to their sensitivity to oxygen and moisture. Polycrystalline samples were prepared using high purity (> 99.9 wt%) elements ($RE=La-Nd$, Sm and Gd ; Li , Sn) purchased from Ames Labs, Alfa, or Aldrich and used as obtained except for Li , which was cleaned free of any dark surface with the aid of a blade. Weighed amounts (totaling ca. 500 mg) of the elements taken in the desired stoichiometric ratio ($RE:Li:Sn=3:4:4$ initially, and then adjusted to 1:1:2 or 1:0.5:2) were filled into Nb tubes, which were arc welded under high-purity Argon gas. The elemental mixtures were then melted by slowly heating them in a high-frequency induction furnace up to 950–1000 °C. The heat treatment was done under residual pressure of 10^{-3} Torr. In all experiments, the temperature was initially raised to 600 °C within 3 h, an intermediate temperature which allows the melting of Sn and Li . The samples were homogenized at the maximum temperature for about 2–4 h, where $T_{max}=950$ °C was used for the $RELi_xSn_2$ ($RE=La-Pr$) samples, and $T_{max}=1000$ °C for the $NdLi_xSn_2$ specimen, respectively. After that the tubes were slowly cooled off at a rate of 5 °C/h for $RELi_xSn_2$ ($RE=La-Pr$), and 10 °C/h for $NdLi_xSn_2$, respectively.

The resulting bulk polycrystalline products were brought in the glove-box, ground using an agate mortar and pestle, and sealed again in Nb tubes for a subsequent heat-treatment following the above-mentioned procedure. After that, the sealed Nb tubes were placed in tube furnaces and annealed at 600 °C over 3–5 days, in order to grow suitable single crystals for the structure determination. The annealed samples were allowed to cool to room temperature by switching off the furnace. The experimental powder X-ray diffraction patterns of the $RELi_xSn_2$ ($RE=La-Nd$) in comparison with the calculated patterns obtained from the single-crystal data revealed > 95 wt% purity of the target phases. Leftover Sn was detected as a minor impurity phase in all cases.

Here, we specifically note that single-crystals of $SmSn_2$ and $GdSn_2$ were first isolated from samples with nominal compositions $SmLiSn_2$ and $GdLiSn_2$. For both samples, the temperature was raised to 950 °C over 2 h, equilibrated for 5 h, followed by a slow cooling (rate of 5 °C/h) to 600 °C, at which temperature the samples were annealed for 1 day. Thereafter, the furnace was switched off.

Besides the above-mentioned reaction schemes, another synthetic approach was also tried to establish the best route to the synthesis of the title compounds. Here, elemental Li and a pre-synthesized binary mixture with nominal composition $RESn_2$ were mixed in equal molar ratios. The materials were loaded into Nb-tubes, which were subsequently encapsulated in fused silica tubes, and flame-sealed upon evacuation. The tubes were then slowly heated at 950 °C, dwelled at this temperature for 5 h and slowly cooled to 600 °C at a rate of 5 °C/h. Finally the samples were cooled to room temperature by switching off the furnace. The powder X-ray diffraction patterns of the as-synthesized samples revealed multi-component mixtures in all cases, although the targets were the major products. This method also confirmed that the $RESn_2$ “precursor” and the “final product” for the reactions involving Sm and Gd are the same.

Caution! Reactions at 950–1000 °C could be dangerous. At these conditions, the Nb tubes and Sn could react, causing Li vapors

(molten metals) to leak into the silica tubes. Therefore, the latter must be made sufficiently long, so that one of the ends can be left protruding outside the furnace. In this way, should a leak occur, a condensation at the end of the silica tube would indicate that the furnace must be stopped immediately.

The crystals of the title compounds are dark grey, with metallic luster. They quickly decompose in air and must be handled with caution. For the purposes of collecting intensity data on the single-crystal diffractometer, the crystals were picked in the glove-box, and covered with Paratone-N oil—the latter was also used as a “glue” in the process of mounting the crystals on the tips of glass fibers.

2.2. Crystallographic studies

X-ray powder diffraction patterns were collected at room temperature on a Rigaku MiniFlex powder diffractometer using filtered $CuK\alpha$ radiation ($\lambda=1.54056$ Å). The diffractometer was enclosed and operated inside a glove-box. The observed peak-positions and the peaks’ relative intensities, analyzed using the JADE 6.5 software package, matched well with those calculated from the single-crystal work. Samples exposed to air for a day lost their crystallinity, and the only Bragg peaks that could be indexed were those of elemental Sn .

Single-crystal X-ray diffraction data were collected on a Bruker SMART CCD-based diffractometer, employing monochromated $MoK\alpha$ radiation ($\lambda=0.71073$ Å) generated from a sealed tube. The operating temperature was 200(2) K, maintained by a cold nitrogen stream. This method for handling the crystals alleviated the issue with their air-sensitivity. After ensuring the crystal quality, full spheres of data were collected in four major sections of frames with 0.4° steps in ω at different θ settings. The typical exposure time was 8–12 s per frame. The whole sphere in reciprocal space was covered up to ca. 56° in 2θ . The Bruker SMART software package [13] was used to process and monitor the data collection. Data reduction and integration, as well as final unit cell refinements were performed using SAINT [14]. Empirical absorption corrections based on equivalent reflections were applied to all data using SADABS [15]. The subprogram XPREP in the SHELXTL [16] software package was used to sort and merge the structure factors as well as to determine the space-group. The systematic extinctions in all data sets proved consistency with the centrosymmetric space group $Cmcm$ (excluding the data for $SmSn_2$, which showed no systematic absences for a c -glide and were merged in $Cmmm$). The structure was solved by direct method using SIR-92 [17] and refined against F^2 using SHELXL-97 [18] as implemented in WinGX [19].

As mentioned already, the crystal structure of $CeLi_xSn_2$ compound was first established, and its atomic coordinates were used as starting model for the refinement of the remaining structures. The structure solution provided three independent crystallographic sites, two of them occupied by $Sn1$ and $Sn2$ atoms, and one by the Ce atoms. The Li atom was assigned on the basis of a peak in the difference Fourier map, distances, and chemical composition. Using these four atoms in the asymmetric unit ($CeNiSi_2$ structure type [5,9]), the first refinement cycles converged to unsatisfactory reliability factors $R_1=12\%$ and $wR_2=30\%$, with three times larger isotropic thermal parameters for the $Sn1$, $Sn2$ and Li atoms (ca. 2.4×10^{-2} Å²) when compared to that of the Ce atom, exhibiting a value of ca. 0.8×10^{-2} Å². Such high atomic displacement parameters are unusual and may be suggestive of defects in the structure (or worse, wrongly assigned positions). More importantly, there was a high residual electron density in the difference Fourier map, indicated by a peak close to $Sn1$. Therefore, in the following trial refinements, the $Sn1$ site was described as a split position $Sn1A$ and $Sn1B$, which lead to an overall improvement of the reliability indices

Table 1
Selected single-crystal data collection and structure refinement parameters for $RELi_xSn_2$ ($RE=La-Nd$).

Empirical formula	$LaLi_{0.69(1)}Sn_2$	$CeLi_{0.63(1)}Sn_2$	$PrLi_{0.56(1)}Sn_2$	$NdLi_{0.44(1)}Sn_2$
Formula weight	381.04	381.85	382.21	384.71
Temperature			200(2) K	
Radiation, λ			MoK α , 0.71073 Å	
Space group, Z			$Cmcm$ (No. 63), 4	
<i>a</i> (Å)	4.5592(13)	4.5123(11)	4.4938(7)	4.4912(4)
<i>b</i> (Å)	18.581(5)	18.234(4)	17.890(3)	17.3844(17)
<i>c</i> (Å)	4.4746(13)	4.4412(10)	4.4251(7)	4.4081(4)
<i>V</i> (Å ³)	379.06(19)	365.41(15)	355.76(9)	344.17(6)
ρ_{cal} (g/cm ³)	6.672	6.961	7.131	7.416
μ (cm ⁻¹)	238.7	255.3	271.2	289.6
Goodness-of-fit on F^2	1.18	1.21	1.30	0.97
Unique reflections	274	265	257	249
Refined parameters	20	20	20	20
R_1 ($I > 2\sigma_I$) ^a	0.0198	0.0287	0.0321	0.0249
wR_2 ($I > 2\sigma_I$) ^a	0.0522	0.0788	0.0838	0.0564
Largest diff. peak and hole ($e^-/\text{Å}^{-3}$)	1.81, -2.74	2.00, -1.83	2.04, -2.19	1.79, -1.41

$$^a R_1 = \sum |F_o| - |F_c| / \sum |F_o|; wR_2 = [\sum [w(F_o^2 - F_c^2)^2] / \sum [w(F_o^2)^2]]^{1/2}, \text{ where } w = 1 / [\sigma^2 F_o^2 + (A \cdot P)^2 + (B \cdot P)], \text{ and } P = (F_o^2 + 2F_c^2) / 3; A, B - \text{weight coefficients.}$$

and no electron density leftover. Next, occupation factors (*sof*) of all atoms were checked—Ce and Sn2 did not deviate from full within 3σ , whereas the refinement with freed *sof* for the Li position revealed significant deficiency (ca. 30–40%). Since Sn1B and Li were both with fractional occupancies and at unrealistically close distance of ca. 2.0 Å, their site occupation factors were restrained to sum up to unity. This, and the constrain on the Sn1A and Sn1B split sites to vibrate with the same displacement parameter produced smoothly converging refinement to satisfactory $R_1=2.8\%$ and $wR_2=7.8\%$ indices, along with more uniform isotropic atomic displacement parameters. We note specifically here that all tested single-crystals isolated from the $RELi_xSn_2$ ($RE=La-Nd$) series revealed the same defect structure and correlation between the refined *sof* of the Li and Sn1B positions. The distance between the two split positions was found to decrease from 0.498(5) Å to 0.409(1) Å for the Ce- and the Nd-analogs, mirroring the decrease of unit cell volumes and the lanthanide contraction [20].

At this stage, it was clear that the originally proposed $CeNiSi_2$ structure type cannot be an acceptable structural model, since split atomic positions (Sn1A and Sn1B) and Li deficiencies must be taken into account. We standardized the positional parameters using the STRUCTURE TIDY program [21] and refined all sites anisotropically (excluding the Li position). The remaining structures were refined using $CeLi_xSn_2$ as a starting model, and all refinements proceeded smoothly. The final difference Fourier maps in all four cases were flat, with highest maxima and minima not larger than $1-2 e^-/\text{Å}^3$.

$SmSn_2$ and $GdSn_2$ structure determinations differed from the above in their own ways. $SmSn_2$ was found to be isotypic with the binary stannides $RESn_2$, which adopt the $ZrGa_2$ structure type with the space group $Cmmm$ [5,10] (also known as $ThGe_2$ or UGe_2 structure type [5]). The structural transformation can also be inferred from the “collapse” of the crystallographic *b*-axis between $NdLi_xSn_2$ ($x=0.44(1)$, Table 1) and $SmLi_xSn_2$ ($x=0$; Table 2). Notice that we report $SmSn_2$ as a binary compound, although the crystal came from a reaction containing Li, and there might be some small amount of Li in it; the crystals obtained from reactions between Sm and Sn only were not adequate for single-crystal work to assert this. We also note that the final difference Fourier map in this case has a small peak of ca. $3 e^-/\text{Å}^3$ located 0.8 Å away from Sm, but it was not possible to include it in any meaningful model for refinements.

The binary $GdSn_2$ phase (space group $Cmcm$, Pearson symbol $oC12$) forms with the $ZrSi_2$ structure type [5,11] and can be viewed as the Li-free version of the $RELi_xSn_2$ structure. As such, there was no disorder found on any of the sites—the Sn1 site behaved

Table 2

Selected single-crystal data collection and structure refinement parameters for $SmSn_2$ and $GdSn_2$.

Empirical formula	$SmSn_2$	$GdSn_2$
Formula weight	387.73	394.63
Temperature		200(2) K
Radiation, λ		MoK α , 0.71073 Å
Space group, Z	$Cmmm$ (No. 65), 4	$Cmcm$ (No. 63), 4
<i>a</i> (Å)	4.4313(14)	4.423(2)
<i>b</i> (Å)	15.768(5)	16.498(3)
<i>c</i> (Å)	4.5221(14)	4.327(2)
<i>V</i> (Å ³)	315.98(17)	315.7(2)
ρ_{cal} (g/cm ³)	8.150	8.302
μ (cm ⁻¹)	337.0	361.3
Goodness-of-fit on F^2	1.17	1.16
Unique reflections	239	233
Refined parameters	15	14
R_1 ($I > 2\sigma_I$) ^a	0.0296	0.0211
wR_2 ($I > 2\sigma_I$) ^a	0.0636	0.0518
Largest diff. peak and hole ($e^-/\text{Å}^{-3}$)	3.22, -1.55	2.14, -1.42

$$^a R_1 = \sum |F_o| - |F_c| / \sum |F_o|; wR_2 = [\sum [w(F_o^2 - F_c^2)^2] / \sum [w(F_o^2)^2]]^{1/2}, \text{ where } w = 1 / [\sigma^2 F_o^2 + (A \cdot P)^2 + (B \cdot P)], \text{ and } P = (F_o^2 + 2F_c^2) / 3; A, B - \text{weight coefficients.}$$

normally, and the only detail worth mentioning is the Sn2 site (the one describing the square-net, vide infra) which displayed large and elongated anisotropic displacement parameter. This appears to be inherent feature of the structure, and is touched upon later.

Selected crystallographic data, atomic coordinates and isotropic-equivalent displacement parameters as well as important interatomic distances for the $RELi_xSn_2$ ($RE=La-Nd$) series, and for the $SmSn_2$ and $GdSn_2$ compounds are gathered in Tables 1–6, respectively. CIFs have also been deposited with Fachinformationszentrum Karlsruhe, 76344 Eggenstein-Leopoldshafen, Germany, (fax: (49) 7247-808-666; e-mail: crysdata@fiz.karlsruhe.de) with depository numbers: CSD-426763 for $LaLi_{0.69(1)}Sn_2$, CSD-426764 for $CeLi_{0.63(1)}Sn_2$, CSD-426765 for $PrLi_{0.56(1)}Sn_2$, CSD-426766 for $NdLi_{0.44(1)}Sn_2$, CSD-426767 for $SmSn_2$, CSD-426768 for $GdSn_2$, and CSD-426769 for $LuSn_2$.

2.3. Electronic structure calculations

The Stuttgart TB-LMTO 4.7 program [12,22] was used to calculate the band structure of an idealized, disorder-free $LaLiSn_2$. The exchange and correlation terms were treated by the local density approximation (LDA) [23]. All relativistic effects except spin orbit coupling were taken into account by using a scalar relativistic approximation [24]. The symmetry of the potential was considered spherical inside each Wigner–Seitz (WS) sphere, and a

Table 3
Atomic coordinates and equivalent isotropic displacement parameters U_{eq}^a for $RELi_xSn_2$ ($RE=La-Nd$).

Atom	Site	x	y	z	Occupancy	U_{eq} (Å ²)
LaLi_{0.69(1)}Sn₂						
La1	4c	0	0.3941(3)	1/4	1	0.0072(2)
Sn1A	4c	0	0.0399(2)	1/4	0.685(6)	0.0103(4)
Sn1B	4c	0	0.0656(3)	1/4	0.315(6)	0.0103(4)
Sn2	4c	0	0.7505(4)	1/4	1	0.0196(3)
Li ^b	4c	0	0.1790(2)	1/4	0.685(6)	0.014(5)
CeLi_{0.63(1)}Sn₂						
Ce1	4c	0	0.3946(3)	1/4	1	0.0053(4)
Sn1A	4c	0	0.0396(2)	1/4	0.628(5)	0.0087(6)
Sn1B	4c	0	0.0668(2)	1/4	0.372(5)	0.0087(6)
Sn2	4c	0	0.7509(6)	1/4	1	0.0179(4)
Li ^b	4c	0	0.1781(2)	1/4	0.628(5)	0.011(6)
PrLi_{0.56(1)}Sn₂						
Pr1	4c	0	0.3955(3)	1/4	1	0.0070(4)
Sn1A	4c	0	0.0402(2)	1/4	0.565(6)	0.0113(6)
Sn1B	4c	0	0.0666(2)	1/4	0.435(6)	0.0113(6)
Sn2	4c	0	0.7510(7)	1/4	1	0.0201(4)
Li ^b	4c	0	0.1802(2)	1/4	0.565(6)	0.014(7)
NdLi_{0.44(1)}Sn₂						
Nd1	4c	0	0.3972(4)	1/4	1	0.0092(3)
Sn1A	4c	0	0.0418(4)	1/4	0.444(11)	0.0134(8)
Sn1B	4c	0	0.0653(4)	1/4	0.556(11)	0.0134(8)
Sn2	4c	0	0.7513(6)	1/4	1	0.0221(4)
Li ^b	4c	0	0.1800(3)	1/4	0.444(11)	0.029(13)

^a U_{eq} is defined as one third of the trace of the orthogonalized U_{ij} tensor.

^b Constrained.

Table 4
Atomic coordinates and equivalent isotropic displacement parameters U_{eq}^a (Å²) for $SmSn_2$ and $GdSn_2$.

Atom	Site	x	y	z	Occupancy	U_{eq} (Å ²)
SmSn₂						
Sm	4j	0	0.14566(6)	1/2	1	0.0098(3)
Sn1	4i	0	0.31575(9)	0	1	0.0124(3)
Sn2	2c	1/2	0	1/2	1	0.0192(5)
Sn3	2a	0	0	0	1	0.0183(5)
GdSn₂						
Gd	4c	0	0.40010(3)	1/4	1	0.0061(3)
Sn1	4c	0	0.06149(5)	1/4	1	0.0107(3)
Sn2	4c	0	0.75130(6)	1/4	1	0.0108(3)

^a U_{eq} is defined as one third of the trace of the orthogonalized U_{ij} tensor.

combined correction was used to take into account the overlapping part. No empty spheres were needed to meet the minimum overlapping criteria. The radii of the WS spheres were determined by an automatic procedure and are as follows: La=2.25 Å, Sn=1.51–1.69 Å and Li=1.25 Å. The basis sets included 6s, 6p, 5d and 4f orbitals for La; 5s, 5p and 5d orbitals for Sn; and 2s, 2p and 3d orbitals for Li. The La 6p and 4f, Sn 5d, and Li 2p and 3d orbitals were treated by the Löwdin downfolding technique [25]. The k-space integrations were done using the tetrahedron method [26], and the self-consistent charge density was obtained with 105 irreducible k-points in the Brillouin zone. The total and partial density of states (DOS), as well as the crystal orbital Hamilton populations (COHP) of selected interactions are presented.

2.4. Magnetic susceptibility measurements

The temperature dependent direct current (dc) magnetic susceptibility data were collected in a Quantum Design magnetic property measurement system (MPMS) SQUID magnetometer under applied magnetic fields of 1000–5000 Oe. Specimens from

Table 5
Selected interatomic distances (Å) in $RELi_xSn_2$ ($RE=La-Nd$).

LaLi_{0.69(1)}Sn₂		CeLi_{0.63(1)}Sn₂	
La1–Sn1A or	3.422(1) × 4	Ce1–Sn1A or	3.386(1) × 4
La1–Sn1B	3.281(1) × 4	Ce1–Sn1B	3.243(1) × 4
La1–Sn1A	3.541(3) × 2	Ce1–Sn1A	3.475(2)
La1–Sn1B	3.919(3) × 2	Ce1–Sn1B	3.868(3) × 2
La1–Li	3.470(9) × 4	Ce1–Li	3.432(2) × 4
La1–Sn2	3.508(1) × 4	Ce1–Sn2	3.459(1) × 4
Sn1A–Li	2.584(3)	Sn1A–Li	2.525(4)
Sn1A–Sn1A	2.683(3) × 2	Sn1A–Sn1A	2.648(3) × 2
Sn1A–La1	3.422(1) × 4	Sn1A–Ce1	3.386(1) × 4
Sn1A–La1	3.541(2) × 2	Sn1A–Ce1	3.475(2) × 2
Sn1B–Li	2.106(3)	Sn1B–Li	2.028(4)
Sn1B–Sn1B	3.309(6) × 2	Sn1B–Sn1B	3.297(6) × 2
Sn2–Li	2.593(2) × 2	Sn2–Li	2.572(2) × 2
Sn2–Li	2.640(2) × 2	Sn2–Li	2.618(2) × 2
Sn2–Sn2	3.194(6) × 4	Sn2–Sn2	3.166(5) × 4
Sn2–La1	3.509(1) × 4	Sn2–Ce1	3.459(1) × 4
PrLi_{0.56(1)}Sn₂		NdLi_{0.44(1)}Sn₂	
Pr1–Sn1A or	3.357(2) × 4	Nd1–Sn1A or	3.320(2) × 4
Pr1–Sn1B	3.2255(9) × 4	Nd1–Sn1B	3.213(1) × 4
Pr1–Sn1A	3.4270(3) × 2	Nd1–Sn1A	3.371(5) × 2
Pr1–Sn1B	3.797(3) × 2	Nd1–Sn1B	3.684(6) × 2
Pr1–Li	3.431(2) × 4	Nd1–Li	3.421(3) × 4
Pr1–Sn2	3.430(1) × 4	Nd1–Sn2	3.394(1) × 4
Sn1A–Li	2.503(4)	Sn1A–Li	2.407(6)
Sn1A–Sn1A	2.639(4) × 2	Sn1A–Sn1A	2.641(78) × 2
Sn1A–Pr1	3.357(2) × 4	Sn1A–Nd1	3.320(2) × 4
Sn1A–Pr1	3.427(3) × 2	Sn1A–Nd1	3.371(5) × 2
Sn1B–Li	2.030(4)	Sn1B–Li	1.999(6)
Sn1B–Sn1B	3.251(6) × 2	Sn1B–Sn1B	3.165(2) × 2
Sn2–Li	2.533(2) × 2	Sn2–Li	2.504(3) × 2
Sn2–Li	2.580(2) × 2	Sn2–Li	2.562(3) × 2
Sn2–Sn2	3.154(4) × 4	Sn2–Sn2	3.1468(2) × 4

Table 6
Selected interatomic distances (Å) in $SmSn_2$ and $GdSn_2$.

SmSn₂		GdSn₂	
Sm–Sn1	3.2236(8) × 4	Gd–Sn1	3.158(1) × 4
Sm–Sn1	3.508(2) × 2	Gd–Sn1	3.461(1) × 2
Sm–Sn2	3.191(1) × 2	Gd–Sn2	3.305(1) × 4
Sm–Sn3	3.223(1) × 2	Gd–Gd	3.943(1) × 2
Sm–Sm	3.967(2) × 2	Sn1–Sn1	2.966(1) × 2
Sn1–Sn1	3.034(2) × 2	Sn2–Sn2	3.094(1) × 4
Sn1–Sn2	3.682(1) × 2		
Sn1–Sn3	3.651(1) × 2		
Sn2–Sn3	3.1657(7) × 4		

at least two different reaction batches were investigated to ensure the reproducibility of the magnetic data. Both field-cooled (FC) and zero-field cooled (ZFC) measurements were carried out in the temperature range of 1.8–300 K. The field dependent magnetization data were gathered at 1.8 K, with applied magnetic field varied between 0 and 70 kOe. All measurements were performed using approximately 50 mg of powdered sample, filled into custom designed sample holders for air-sensitive materials [27]. The holder contribution was subtracted from the raw magnetization data, which were subsequently converted to molar susceptibility.

3. Results and discussion

3.1. Synthesis and chemical formulae

Two different synthetic approaches were used to establish the best route toward single-phase product of the $RELi_xSn_2$ compounds. The

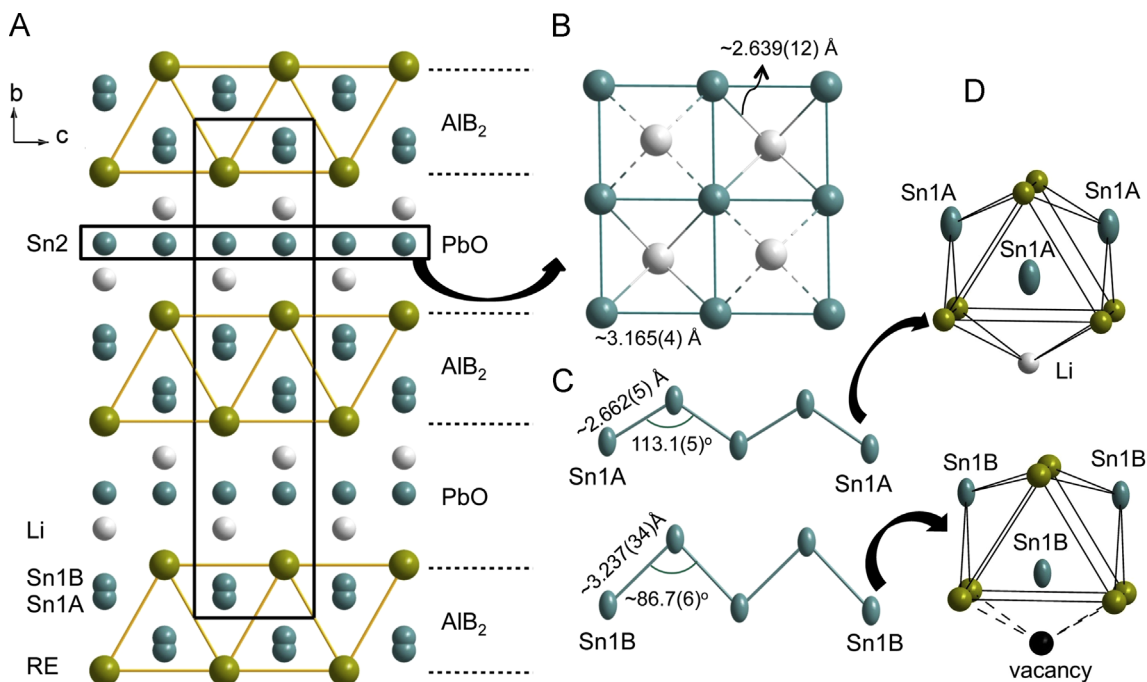


Fig. 1. (A) Projection of the crystal structure of $RELi_xSn_2$ ($RE=La-Nd$) along the a -axis showing intergrowth sequences of AlB_2 -like and PbO -like slabs. (B) Top view along $(0\ 1\ 0)$ of the planar square nets capped alternatively above and below with Li atoms. (C) Cutouts of the 1D $Sn1A$ and $Sn1B$ zigzag chains exhibiting different bond lengths and angles. (D) Coordination polyhedra for the $Sn1A$ and $Sn1B$ atoms.

first method employed 1:1:2 mixtures of RE , Li and Sn —as suggested from the powder X-ray diffraction patterns, which are in excellent agreement with the simulations, the target materials can be produced in high yields. Nevertheless, there remain some minor impurity peaks that could not be assigned to a known phase. In all cases, the single-crystal structure refinements revealed a non-stoichiometric $RELi_xSn_2$ ($x \approx 0.4-0.7$), i.e., with Li deficient composition. This is in agreement with the literature, where among the many isostructural compounds MT_xX_2 ($0 < x \leq 1$; M is an alkaline-earth or rare-earth metal, T stands for transition metal, and $X=Si, Ge, \text{ or } Sn$) [5], only very few are fully stoichiometric. Examples here include $BaCuSn_2$ [27], $SrCuSn_2$ [28], $CaNiGe_2$ [29], and $SrNiGe_2$ [30], while a relatively much larger number crystallize with significant amounts of vacancies at the T sub-lattice, especially among the stannides [5,31–33].

The above suggests that the $RELi_xSn_2$ compounds inherently exist within a certain homogeneity range and may never form in the fully lithiated form. We acknowledge that the homogeneity range may be varied beyond the reported limits with the annealing temperature, which in our case is $600^\circ C$ (vs the $200^\circ C$ annealing temperature in the original study by Pavlyuk et al. [4]), but since the nominal compositions were Li -rich, we could argue that $x_{max} \approx 0.7$ as seen for $LaLi_{0.69(1)}Sn_2$ represents the highest amount of Li uptake in this structure. The Li content x was found to decrease gradually (Table 1) with the decreasing size of the lanthanide atoms ($r_{La}=1.69$ Å, $r_{Ce}=1.65$ Å, $r_{Pr}=1.64$ Å, $r_{Nd}=1.63$ Å) [34], which is an important structural trait related to the unit cell volume and the “available” space for lithiation within the $RESn_2$ sub-structure.

The minimal solubility limit x_{min} was not probed, however, it cannot be expected that a continuous solid solution $RELi_xSn_2$ ($0 < x_{min} \leq x \leq x_{max}$) will exist—after all, the end members $RESn_2$ with the $ZrSi_2$ structure type [5,11] do not exist for the light rare-earth metals (they are known for Gd through Lu only) [6–8]. Furthermore, there are several closely related RE_nSn_{3n-2} phases [7] (e.g., $RESn_2$ for $n=2$, which is the same as $SmSn_2$ with the $ZrGa_2$ structure type [5,10], elaborated later on in the text).

The second approach for the synthesis of the $RELi_xSn_2$ phases emphasizes the use of a binary $RESn_2$ precursor. The goal here was not only to target higher quality single-phase samples, but also to gain some insights on the possible homogeneity ranges. Though this method also enabled small single-crystals of the desired compounds, their quality was inferior, and the structural work was challenging and unsuccessful. No overall improvement of the phase purity could be obtained after repeated heating cycles.

3.2. Structure

As mentioned above, the $RELi_xSn_2$ ($RE=La-Nd$) compounds crystallize with the space group $Cmcm$ (no. 63). All five crystallographically independent positions in the asymmetric unit are located on Wyckoff sites $4c$ and have site symmetry $m2m$ (Fig. 1). Formally, this arrangement constitutes a defect version of the $CeNiSi_2$ structure (Pearson code $oC16$) [5,9], or conversely, a partially filled version of the $ZrSi_2$ structure (Pearson code $oC12$) [5,11]. In this work, using our single-crystal data, we show that the Li atoms in the structure are responsible for some Sn disorder, modeled by splitting the $Sn1$ atomic position to $Sn1A$ and $Sn1B$ (same multiplicity).

We note that the earlier crystallographic data claiming $RELiSn_2$ for $RE=La-Lu$ show highly unusual variation of the unit cell parameters [4]. Specifically, it has been reported that the b -axis is invariant of the size of the rare-earth metals, while the a - and c -axis marginally decrease across the series. Overall, the decrease of the unit cell volumes follows the lanthanide contraction, but the data as a whole is inconsistent with our findings—we report unit cell contraction in all three directions (Table 1). With the Sm -compound, the dependence of the unit cell volume on the lanthanide size abruptly changes slope, indicative of a structural change. The variation in the unit cell volumes between $SmSn_2$ and $GdSn_2$ is miniscule, because of yet another structural rearrangement (Table 2). From $GdSn_2$ on, the structure is retained until $LuSn_2$ (with the exception of $YbSn_2$ which does not exist) [6–8],

whereby the unit cell axes/volumes decrease monotonically. This has been established by landelli and Palenzona [6], and confirmed by the single-crystal structures of GdSn₂ (Table 2) and LuSn₂ (Supporting information).

The idealized, disorder-free structure can be articulated as intergrowth of AlB₂- and PbO-like slabs [5]. The Sn1 atoms form $\frac{1}{\infty}$ [Sn₂] zigzag chain within a layer of fused trigonal prisms of RE, an arrangement which is the hallmark of the AlB₂ structure type [5]. The Li and Sn2 atoms form PbO-like slabs, where each Sn atom is in a tetrahedral environment of Li atoms (Fig. 1A). The Li position shows occupational disorder, which correlates with the positional disorder involving the neighboring zigzag chain—the Sn1 site splits into two distinct Sn1A and Sn1B positions. A simultaneous occupation of Sn1A and Sn1B is not allowed due to the unphysical distance between them (ca. 0.4–0.5 Å). The same holds true for the Li and Sn1B positions (distance ca. 2.0–2.1 Å). Therefore, Li and Sn1B are treated as mutually exclusive.

If we consider the zigzag chain made of Sn1A only, the Sn1A–Sn1A distances vary between 2.683(3) and 2.641(8) Å, and the Sn1A–Sn1A–Sn1A angle ca. 113.2° (Fig. 1C), almost invariant of the unit cell contraction between LaLi_{0.69(1)}Sn₂ and NdLi_{0.44(1)}Sn₂. The Sn1B–Sn1B interatomic distances vary in the range 3.309(6)–3.165(2) Å, and the Sn1B–Sn1B–Sn1B angle decreases slightly from 88.3(4)° to 85.09(2)° between the La- and Nd-analogs. The longer bonds and the more “kinked” topology of the Sn1B zigzag chain (i.e., no Li atom present) means that the Sn1B atom comes closer to its Sn2 neighbor from the square net, probably allowing some indirect interaction to compensate for the empty space [35].

The Sn1A atoms take the position near the center of trigonal prisms of RE atoms, having two Sn1A, and one Li atoms capping the rectangular faces (Fig. 1D). The Sn1A–Li distances are reasonable, ca. 2.6 Å, but shorter when compared to the sum of the covalent radii between the Li and Sn atoms (~2.9 Å) [34], which may be suggestive of much larger displacement of the Li atoms. Sn–Li distances as short as ca. 2.7 Å are reported in some binary compounds such as Li₁₇Sn₄ [36], LiSn [37], and Li₂Sn₅ [38].

Concerning the Sn1A/Sn1B–RE distances, there appear to be no unphysically short contacts due to the disorder/offsetting of the Sn1 atom. The Sn1A–RE distances are distributed over the ranges 3.422(1)–3.320(2) Å and 3.541(3)–3.371(5) Å, respectively, on passing from LaLi_{0.69(1)}Sn₂ to NdLi_{0.44(1)}Sn₂ (Table 5). The corresponding Sn1B–RE distances fall in the intervals 3.281(1)–3.213(2) Å and 3.916(6)–3.686(6) Å, respectively. For comparison, the Sn2–RE contacts vary between 3.509(1) Å and 3.394(1) Å as the size of the rare-earth decreases from La to Nd within these structures.

The PbO-like slabs feature planar square nets of Sn2 atoms, capped above and below (alternatively) by the Li atoms (Fig. 1B) to form puckered [Li_xSn₂] layers propagating along the *ac*-plane. Each Sn2 atom is coordinated by four other Sn2 atoms with Sn2–Sn2 distances ranging from 3.1941(6) Å to 3.1468(2) Å on going from the La- to the Nd-analog. These distances are considerably longer than the averaged Sn1A/B–Sn1A/B distance and the Sn–Sn distance in α -Sn (4×2.81 Å) [20]. These values match the contacts in the metallic β -Sn (4×3.02 and 2×3.18 Å) [20], suggesting weaker covalent interactions between the Sn2 atoms. Papoian and Hoffmann had analyzed in detail this scenario, dubbed as hypervalent bonding [35]—such configuration may favor a distortion leading to breaking or puckering of the Sn2 sheets. Interestingly, we found elongated anisotropic displacement parameters U_{22} ($\sim 2.3 \times 10^{-2}$ Å² from averaging the U_{22} values in Table S1 in Supplementary information) for the Sn2 atoms suggesting a possible small Peierls distortion transforms these hypervalent square nets into classical structures with reduced dimensionality (such as closely spaced zigzag chains the *ac*-plane) [35]. However, there were no satellite reflections present in the gathered X-ray data, which could indicate superstructures or lowered symmetry due to ordering of the Li vacancies and/or breaking the $\frac{2}{\infty}$ [Sn₂] square nets

(a recent example of a modulated superstructure where this has been observed is the structurally related TbFe_{0.25}Ge₂ [39]).

There are two distinct Sn2–Sn2–Sn2 angles, which are almost invariant of the unit cell metrics, and measure around 88.9° and 91.1°. The Li atom that caps the Sn layer is located at distances ca. 2.5–2.6 Å. These shortened distances attest for the “crowdedness” of the structure and help explain the gradual decrease of the Li content with the lanthanide contraction—likely, the “free volume” within the RESn₂ sub-structure is not sufficient for a complete lithiation without additional structural distortion. To evaluate this hypothesis, we re-plotted the structure in a way that emphasizes the distribution, packing and connection of RE/Sn polyhedra, centered by the Li atoms (Fig. 2). Their volumes, as well as the volumes of the Voronoi cells were calculated with the aid of the NRCVAX software package [40]. As expected, between LaLi_{0.69(1)}Sn₂ and NdLi_{0.44(1)}Sn₂, the volumes of these partially filled trigonal prisms, were found to decrease from 62.96 Å³ to 57.66 Å³, and the volumes of the Voronoi cells to decrease from 19.64 Å³ to 17.71 Å³, respectively. These results are consistent with the observed reduction of the *b*-axis, and bolster the supposition that stoichiometric RELiSn₂ phases, as reported in the literature [4], are unlikely, even with the very early lanthanides. Further, because of the quickly diminishing volumes, Li uptake falls off rapidly, and it is very plausible that RELi_xSn₂ cannot be formed with the mid-to-late rare-earth metals; instead the Li-free RESn₂ (RE=Gd–Lu) exist.

3.3. Structures of SmSn₂ and GdSn₂

The RELi_xSn₂ series appears to end with RE=Nd, and for RE=Sm, the same structure could not be realized. Instead, the binary SmSn₂ phase (Fig. 3—ZrGa₂ structure type, space group *Cmmm*, Pearson symbol *oC12*) [5,10] was formed. The nonidentical divalent Eu afforded only EuSn₃ [41], and another, yet unidentified product, while for RE=Gd, the major product of the Gd–Li–Sn reaction was the binary GdSn₂ phase (Fig. 4—ZrSi₂ structure type, space group *Cmcm*, Pearson symbol *oC12*) [5,11].

SmSn₂ had been previously reported from powder X-ray diffraction data as part of the study on the RE_nSn_{3n–2} homologous series by Rogl et al. [7]. GdSn₂ had been previously identified, also from its powder X-ray diffraction pattern by landelli and Palenzona [6]. The unit cell volumes for SmSn₂ and GdSn₂ from the literature are in good, but not perfect agreement with ours (Table 2). Advances in the quality of rare-earth metals and/or differences in the diffraction equipment are among the most likely reasons for the observed discrepancies. Here, we re-evaluate the two structures on the basis of single-crystal work and provide more accurate atomic coordinates, displacement parameters, and distances.

The structure of SmSn₂ is described by four crystallographically independent positions with different site symmetries (Table 4). The Sn1 atoms form $\frac{1}{\infty}$ [Sn₂] zigzag chains along the *a*-axis (Fig. 3A). A cutout of the zigzag chain is shown in Fig. 3B. The Sn1–Sn1 distance of 3.035(2) Å is slightly smaller compared to the distance of 3.22 Å reported in the literature [7]. The Sn1–Sn1–Sn1 angle of 93.823(5)° also differs from the reported angle (86.63°). The zigzag chains alternate with layers of $\frac{2}{\infty}$ [Sn₂] square nets, which are formed by Sn2 and Sn3 atoms with Sn2–Sn3 distance of 3.1657(7) Å. Note that because of the significant contraction of the *b*-axis, one might consider the zigzag chains and the square nets as “merged” with Sn1–Sn2 and Sn1–Sn3 distances of 3.682(1) Å and 3.651(1) Å (vertical separation between them of only 2.906 Å!). Taking this into consideration, an alternative description of the structure emerges—layers of elongated, vertex-shared [Sn₆] octahedra alternating with layers of Sm atoms. As discussed by Rogl and co-workers [7], this structure is an early member of the

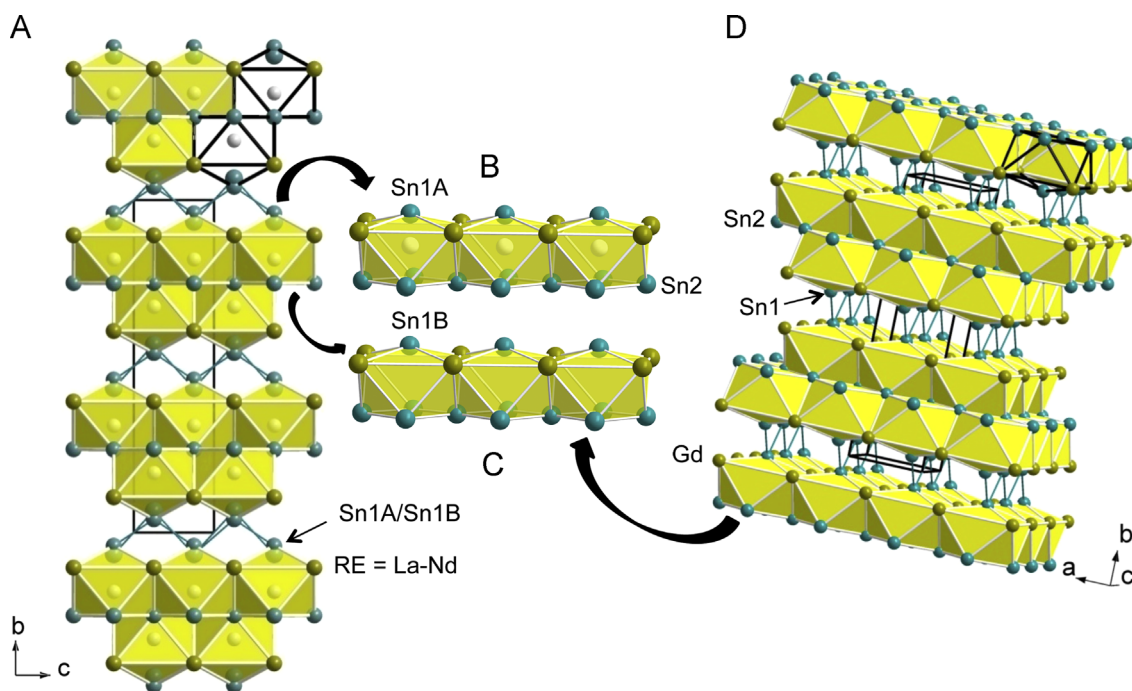


Fig. 2. The relationship between the crystal structure of $GdSn_2$ and $RELi_xSn_2$ ($RE = La-Nd$), which are its Li-filled analogs. (A) Projection of the structure of $RELi_xSn_2$ ($RE = La-Nd$) articulated as a space filling of layers of edge-sharing tricapped trigonal prisms interconnected via Sn1A–Sn1A or Sn1B–Sn1B bonds. The $RE-Sn1$ contacts are omitted for clarity. (B) The occupation of original Sn1 position by the Sn1A atoms leads to a sequence of filled $\{Li\}RE_4(Sn2)_2$ trigonal prisms (i.e., an idealized $CeNiSi_2$ -type arrangement). (C) A sequence of empty trigonal prisms is modeled with the Sn1B atoms due to short Li–Sn1B contacts, leading to an atomic arrangement similar to that of the structure of $GdSn_2$ depicted in panel (D). The structure of these new compounds can be therefore considered as intermediate between the $CeNiSi_2$ and $ZrSi_2$ structures.

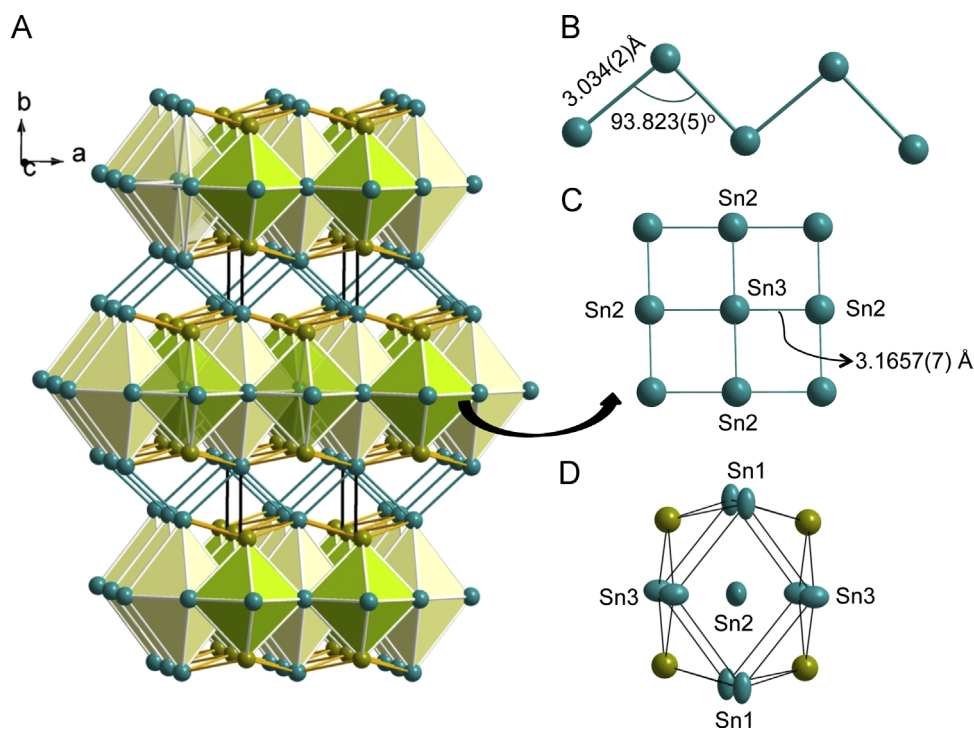


Fig. 3. (A) The crystal structure of $SmSn_2$ viewed along the c -axis. (B) Cutout of the 1D Sn1 zigzag chain; (C) top view projection along the b -axis of the planar square nets; (D) coordination polyhedron of Sn2 atoms featuring displacement of the Sn1 atoms along $(0\ 1\ 0)$, Sn3 atoms along $(1\ 0\ 0)$ and Sn2 atoms along $(0\ 0\ 1)$.

RE_nSn_{3n-2} homologous series, which starts with $RESn$ (orthorhombically distorted CsCl structure type, $n=1$) and ends with $RESn_3$ ($AuCu_3$ structure type, $n=\infty$), where the vertex-shared $[Sn_6]$ -octahedra are extended in a 3D-structure. This crystal chemistry also bears resemblance with the perovskites, and with the layered structures of the Ruddleson–Popper phases [42].

We must also note that analysis of the anisotropic displacement parameters (U_{ij}) given in [Supplementary information \(Table S2\)](#) revealed that the U_{22} ($2.24 \times 10^{-2} \text{ \AA}^2$) for Sn1, U_{33} ($2.86 \times 10^{-2} \text{ \AA}^2$) for Sn2 and U_{11} ($2.86 \times 10^{-2} \text{ \AA}^2$) for Sn3 are slightly enlarged, which induces a change from their ellipsoids shape-like to prolate ellipsoids directed towards $(0\ 1\ 0)$, $(0\ 0\ 1)$,

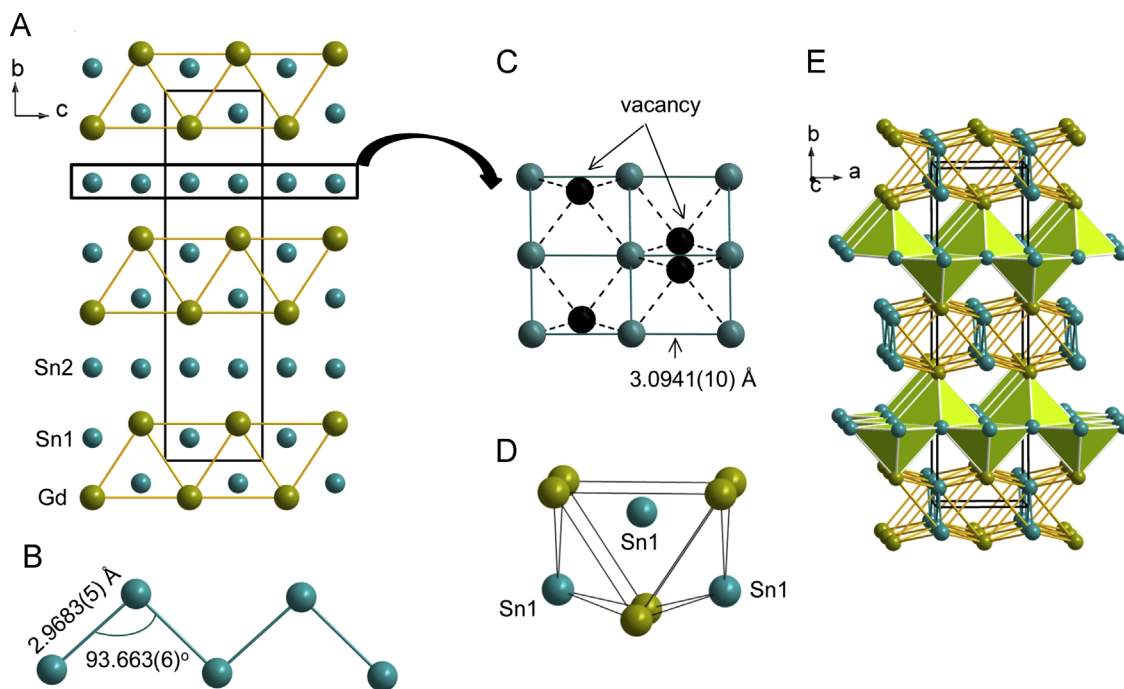


Fig. 4. (A) Projection of the crystal structure of GdSn_2 , viewed along the a -axis. (B) Cutouts of the Sn1 zigzag chains; (C) top view along (0 1 0) of the planar square nets capped alternatively above and below with the Gd atoms; (D) coordination polyhedra for the Sn1 atoms (CN8). (E) Crystal structure of GdSn_2 viewed along the c -axis, described as stacking of alternated layers of $\{\text{RE}\}(\text{Sn}_2)_4$ pyramidal units and Sn1 zigzag chains running along (0 1 0).

and (1 0 0) planes, respectively (Fig. 3D). These unusual anisotropic displacement parameters may be suggestive of intrinsic structural defects that need further investigation. The Sm–Sn distances (Table 6) fall in the range of 3.191(1)–3.508(2) Å, matching well those (3.185–3.572 Å) from the earlier powder data [7].

The structure of GdSn_2 contains 3 atoms per asymmetric unit, distributed over Sn1, Sn2, and Gd sites with the same local symmetry. The Sn1 atoms in GdSn_2 form the zigzag chains (Fig. 4), aligned along the c -axis. The refined Sn1–Sn1 distances are 2.9683(5) Å, slightly shorter when compared to those (3.094 Å) calculated from powder data [6]. We can also compare the Sn1–Sn1 distances in the isotypic LuSn_2 , also refined from single-crystal data (2.959(1) Å, see Supporting information), which shows that the lanthanide contraction and the corresponding unit cell volume change has a small effect on the Sn1–Sn1 bonding. This also underscores the importance of refining structures, even when the work may appear redundant. This point is particularly well illustrated by comparing the Sn2–Sn2 bond length within the ${}^2_\infty[\text{Sn}_2]$ square nets—refined value of 3.094(1) Å, vs 3.037 Å, reported from the early work [6] ($d_{\text{Sn}_2-\text{Sn}_2}=3.0323(8)$ Å in LuSn_2 , see Supporting information). The Sn2 bonds appear to be more sensitive to the volume change from GdSn_2 to LuSn_2 , the planar square nets in the RELi_xSn_2 ($\text{RE}=\text{La}-\text{Nd}$) series (Table 5) are even more expanded. The shortest Gd–Sn contacts occur between Gd and Sn1 and vary from 3.158(1) Å to 3.461(1) Å.

Last, we briefly compare the structures of GdSn_2 and SmSn_2 . The basic building blocks here are nearly identical, the valence electron counts are the same. What are the differences? The Sn–Sn distances with the zigzag chains and the square nets are proportional to the atomic sizes of Sm and Gd, so are the Sm–Sn and Gd–Sn distances. The most notable distinction is the vertical separation between the zigzag chains and the square nets—as mentioned already, the short separation in SmSn_2 allow for a structure description in terms of elongated, vertex-shared $[\text{Sn}_6]$ -octahedra. In GdSn_2 , the zigzag chains and the square nets are 3.131 Å away, and even in LuSn_2 , they are still further apart (2.982 Å) than in SmSn_2 . This might be the signature of an obscure, but important

interaction that overrides the apparent electronic instability of the structure (vide infra). Further evidence supporting this line of thinking comes from comparing the isostructural, but not isoelectronic GdSn_2 (11 valence electrons per formula unit) and ThSn_2 (12 valence electrons per formula unit) [43]. Note that the ionic radii for the Gd^{3+} and Th^{4+} ions are nearly identical (CN 8, $r(\text{Gd}^{3+})=1.193$ Å; $r(\text{Th}^{4+})=1.19$ Å [44]), yet, in the ThSn_2 structure the vertical separation between the zigzag chains and the square nets is almost 0.13 Å larger at 3.257 Å, in spite of the very similar Th–Sn and Gd–Sn distances. This “oxidation” of the square nets, where the formal electron counts change from the electronically saturated $(\text{Th}^{4+})({}^1_\infty[\text{Sn}_2]_{2-})({}^2_\infty[\text{Sn}_2]_{2-})$ to $(\text{Gd}^{3+})({}^1_\infty[\text{Sn}_2]_{2-})({}^2_\infty[\text{Sn}_2]_{1-})$ has already been discussed in the review by Papoian and Hoffmann [35] on hypervalent bonding in chains and sheets formed by the light and the heavy groups 14, 15 and 16 elements.

3.4. Electronic structure

Having just mentioned the valence electron count in GdSn_2 and ThSn_2 is a perfect way to begin the discussion on the electronic structure. Note that based on the formal charges, all Li-free RESn_2 ($\text{RE}=\text{Gd}-\text{Lu}$) phases will have less than optimal electron count, since the ideal valence electron count for square sheet of Sn atoms is $6 e^-/\text{atom}$ [35], and it cannot be met if the cation is a trivalent rare-earth metal (vide supra). This has been previously discussed elsewhere [35], and our tight-binding linear-muffin-tin-orbital (TB-LMTO-ASA) electronic structure calculations for LuSn_2 (supporting information) confirm that the Fermi level is indeed located in a region of relatively high DOS. Just above it, a deep pseudo gap indicates that an electron-richer structure could be electronically more stable. This would be the case for an idealized LaLiSn_2 , where one more electron from the inserted Li atom restores the optimal valence electron count.

The TB-LMTO-ASA electronic structure calculations for a model LaLiSn_2 (coordinates and unit cell dimensions from $\text{LaLi}_{0.69(1)}\text{Sn}_2$, with the occupancy of Li assumed to be full, and the Sn1 splitting neglected) confirm this reasoning. The plots of the computed

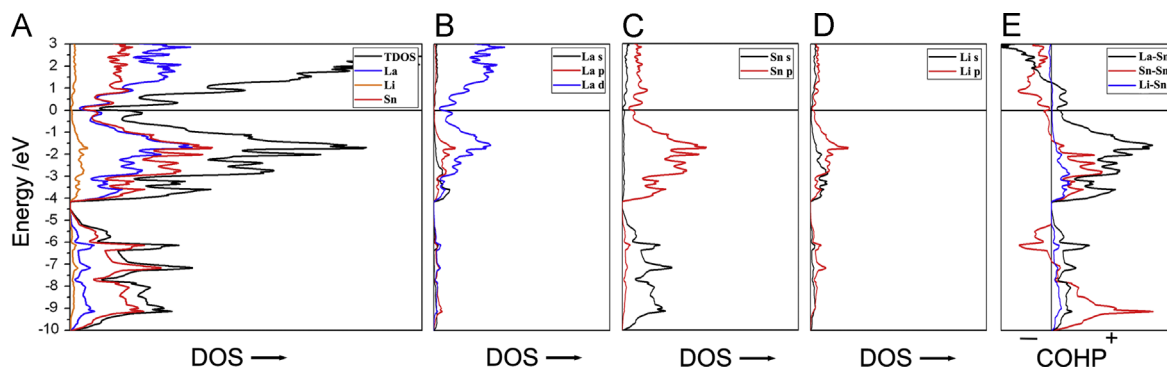


Fig. 5. (A) Calculated DOS diagrams for LaLiSn₂. The Fermi level is set as the energy reference at 0 eV. (B) Partial DOS curves for *s*, *p*, *d* bands of La. (C) Partial DOS curves for *s*, *p* bands of Sn. (D) Partial DOS curves for *s*, *p* bands of Li. (E) Integrated COHP curves of the La–Sn, Li–Sn, and Sn–Sn interactions. Since the “inverted” COHP values are plotted, the positive regions represent the bonding interactions, while the negative regions denote antibonding interactions.

density of states (DOS) and the crystal orbital Hamilton populations (COHP) are shown in Fig. 5. In the total DOS diagram (Fig. 5 (a)), there is no band gap between the valence band and conduction band, which suggests the metallic behavior of LaLiSn₂. The Fermi level (solid line) is located in a region of relatively low DOS (pseudo gap), indicating favored electronic structure. The bands in the DOS curve can be separated into two energy ranges. Below the Fermi level from 0 eV to –4 eV, the contributions of the bands are mainly from La 5*d* and Sn 5*p* bands, where in the range from –5 eV to –10 eV, the major part of the DOS is from the Sn 5*s* band. In both energy ranges, significant overlapping of the bands from La, Li and Sn indicates strong bonding interactions between the atoms of these elements. This is a typical feature of the polar intermetallics, in which the covalency of the interaction between the presumed “cations” and “anions/polyanions” is very important for the overall electronic stability. The results are in excellent agreement with previous studies on this structure [24,31–33,35].

According to the COHP curves (Fig. 5(e)), at the Fermi level, the La–Sn interactions are in bonding states, while the Sn–Sn ones are in anti-bonding states. The Li–Sn interactions are also nearly optimized, which suggests strong covalency between Li and Sn atoms. The anti-bonding Sn–Sn states are fully compensated by the La–Sn interactions, and removing electrons from the anti-bonding regions (emptying hypervalent bands) appears to have little structural consequences. In fact, lowering the Fermi level to the pseudo-gap slightly below (ca. –0.4 eV) confirm the experimental results that the RELi_{*x*}Sn₂ (*RE*=La–Nd) compounds do not exist with full lithium filling. Assuming the rigid band model is valid, the shifted Fermi level will correspond to integrated 11.6 valence electrons (formula LaLi_{0.6}Sn₂), which agrees well with the refined composition. However, the variations in the Li uptake with the sizes of the rare earth metals suggest that geometric factors, as discussed above, may take priority over the electronic reasons for stability with near 12 valence electrons/f.u., calling for more experimental/ theoretical studies of these compounds, and the structure type in general.

3.5. Magnetism

Fig. 6 shows the temperature dependence of the molar magnetic $\chi(T)$ and the inverse molar magnetic susceptibility $\chi^{-1}(T)$ of the RELi_{*x*}Sn₂ (*RE*=Ce–Nd) series. As the temperature increase above 100 K, the $\chi^{-1}(T)$ plot follows well the Curie–Weiss law $\chi(T) = C/(T - \theta_p)$ [45], where θ_p is the paramagnetic Weiss temperature and *C* is the Curie constant defined as $C = \mu_0 \mu_{\text{eff}}^2 / 3k_B$, where $\mu_0 = 4\pi \times 10^{-7} \text{ H m}^{-1}$ is the permeability of the vacuum, μ_{eff} stands for the effective magnetic moment, and $k_B = 1.38 \times 10^{-23} \text{ J K}^{-1}$ is the Boltzmann constant. The effective magnetic moments derived from the linear fits of the inverse susceptibility are

$2.61 \mu_B$ ($g_J[J(J+1)]^{1/2} = 2.54 \mu_B$) for the Ce, $3.56 \mu_B$ ($g_J[J(J+1)]^{1/2} = 3.58 \mu_B$) for the Pr, and $3.61 \mu_B$ ($g_J[J(J+1)]^{1/2} = 3.62 \mu_B$) for the Nd-compound, respectively. As compared to the free-ion moments from the Hund’s rule [45] (given in parentheses, in which *g* is the Landé factor and *J* stands for the total angular momentum of the 4*f*-shell), the estimated effective magnetic moments are very close, indicating the well-localized nature of the 4*f*-electrons in all three cases. The numbers also confirm the expected 3⁺ ground states for Ce, Pr, and Nd.

The paramagnetic Weiss temperatures, θ_p , for all samples were found to be positive and gradually decreasing from 12 K to 2 K on passing from CeLi_{0.63(1)}Sn₂ to PrLi_{0.56(1)}Sn₂ to NdLi_{0.44(1)}Sn₂. The positive values of θ_p for all three samples indicate that the magnetic interactions in the paramagnetic regime are of ferromagnetic type. These findings in part contradict the results from the original study by Pavlyuk et al. [4], where the Ce- and Pr-samples had negative Weiss temperatures ($\theta_p = -17 \text{ K}$ and $\theta_p = -3 \text{ K}$), while the Nd-analog had $\theta_p = 2 \text{ K}$, matching our data. The earlier measurements did not allow for measurements at sufficiently low temperatures to capture the onset of spontaneous magnetic ordering, while others do—the magnetic ordering temperatures (T_C) calculated from the mid-point of jump in the $\chi(T)$ curves are close to 8–9 K for the Ce- and Pr-samples and almost 15 K for the Nd-sample. Fig. 6D displays the dependence of both θ_p and T_C with the De Gennes factor $(g-1)^2 J(J+1)$ [45], which clearly suggest that the magnetic response of these materials is not trivial. Further experimental data backing up this conjecture are the divergent ZFC and FC curves for PrLi_{0.56(1)}Sn₂ and NdLi_{0.44(1)}Sn₂ (see Supporting information), which could indicate metamagnetic behavior similar to that of PrSn₂ (ZrGa₂ type), which at low field appears to be an antiferromagnet like its PrSn₂ counterpart [7], but at higher applied fields shows parallel alignments of the Pr-moments. We can also cite here the refinements from neutron diffraction for the binary phases with the heavy rare-earth metals RESn₂ (*RE*=Tb–Tm) [8], which show the existence of sine-modulated magnetic structures undergoing successive transitions to collinear antiferromagnetically ordered states at lower temperatures. Given this level of complexity, we are preparing for field-dependent measurements, as well as ac-magnetometry and neutron diffraction investigations, which are needed to clarify the behavior of the RELi_{*x*}Sn₂ (*RE*=Ce–Nd) samples.

4. Conclusions

The crystal structures of the RELi_{*x*}Sn₂ (*RE*=La–Nd, Sm, Gd; $0 \leq x < 1$) compounds have been revised on the basis of single-crystal X-ray diffraction data. We have shown that these compounds crystallize with the defect CeNiSi₂ structure, within which

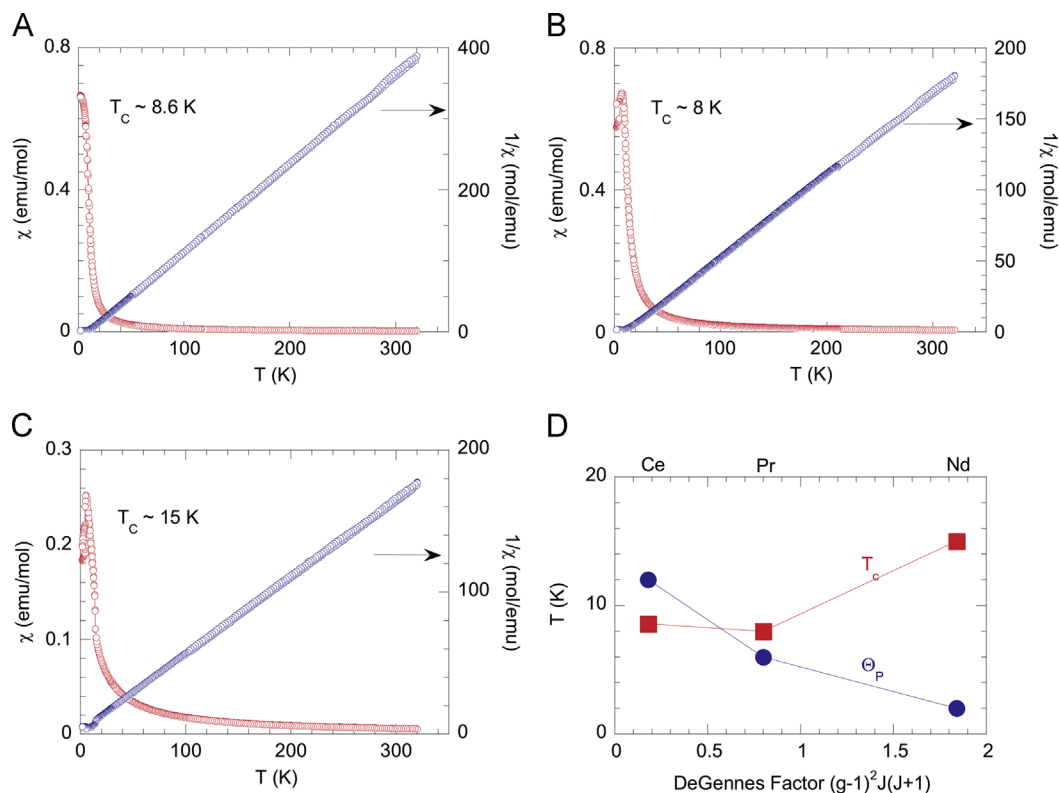


Fig. 6. Magnetic susceptibility vs temperature for polycrystalline CeLi_{0.63(1)}Sn₂ (A), PrLi_{0.56(1)}Sn₂ (B), and NdLi_{0.44(1)}Sn₂ (C). The inverse susceptibilities and how they vary with the temperature are also shown. Panel (D) shows the T_c and θ_p variations with the deGennes factors for the 3 measured samples. ZFC and FC data are overlaid and the only places where divergence is observed, are the data at the lowest temperature for PrLi_{0.56(1)}Sn₂ (B), and NdLi_{0.44(1)}Sn₂ (C). We refer the reader to the online Supporting Information for magnified views of the low temperature regions.

the Li positions feature significant deficiencies leading to a large displacement of the Li atoms along the b -axis. Consequently, the Li–Sn1 interactions are shortened, causing a split atomic position Sn1A and Sn1B. The Li deficiency and the refined occupation factor of the Sn1B atoms were found to increase monotonically with the decreasing size of the rare earth atoms. This led to intricate pattern of correlated disorders between these two atomic positions. The present study did not find any evidence for the existence of modulated superstructures, which might be possible for some compositions within the reported homogeneity range. Further investigations are awaited to clarify this behavior.

Acknowledgments

Svilen Bobev acknowledges financial support from the National Science Foundation through a grant DMR-0743916 (CAREER).

Appendix A. Supplementary materials

Supplementary data associated with this article can be found in the online version at <http://dx.doi.org/10.1016/j.jssc.2013.12.010>.

References

- [1] S. Bobev, T.-S. You, N.-T. Suen, S. Saha, R. Greene, J.P. Paglione, *Inorg. Chem.* 51 (2012) 620.
- [2] S.-P. Guo, T.-S. You, S. Bobev, *Inorg. Chem.* 51 (2012) 3119.
- [3] S.-P. Guo, T.-S. You, Y.-H. Jung, S. Bobev, *Inorg. Chem.* 51 (2012) 6821.
- [4] V.V. Pavlyuk, O. Bodak, V. Pecharskii, R. Skolozdra, E. Gladyshevskii, *Inorg. Chem. Mater.* 25 (1989) 1145.

- [5] P. Villars, L.D. Calvert (Eds.), *Pearson's Handbook of Crystallographic Data for Intermetallic Compounds*, second ed., American Society for Metals, Materials Park, OH, USA, 1991. (and the desktop edition 1997).
- [6] A. Iandelli, A. Palenzona, G.B. Bonino, *Atti Accad. Naz. Lincei Cl. Sci. Fis. Mat. Nat. Rend* 40 (1966) 623.
- [7] F. Weitzer, K. Hiebl, P. Rogl, *J. Solid State Chem.* 98 (1992) 291.
- [8] G. Venturini, P. Lemoine, B. Malaman, B. Ouladidif, *J. Alloys Compd* 505 (2010) 404.
- [9] O.P. Bodak, E.I. Gladyshevskii, *Sov. Phys. Crystallogr* 14 (1970) 859.
- [10] M. Pötzschke, K. Schulbert, *Z. Metallkunde* 53 (1962) 474.
- [11] H. Schachner, H. Nowotny, H. Kudielka, *Monatsh. Chem.* 85 (1954) 1140.
- [12] H.L. Skriver, *The LMTO Method*, Springer, Berlin, 1984.
- [13] SMART, Bruker AXS Inc., Madison, Wisconsin, USA, 2003.
- [14] SAINT, Bruker AXS Inc., Madison, Wisconsin, USA, 2003.
- [15] SADABS, Bruker AXS Inc., Madison, Wisconsin, USA, 2003.
- [16] SHELXLT, Bruker AXS Inc., Madison, Wisconsin, USA, 2003.
- [17] A. Altomare, G. Cascarano, C. Giacovazzo, A. Guagliardi, M.C. Burla, G. Polidori, M. Camalli, *J. Appl. Crystallogr* 27 (1994) 435.
- [18] G.M. Sheldrick, *Acta Crystallogr. A* 64 (2008) 112.
- [19] L.J. Farrugia, *J. Appl. Cryst.* 32 (1999) 837.
- [20] J. Donohue, *The Structures of the Elements*, Wiley, New York, USA, 1974.
- [21] L.M. Gelato, E. Parthé, *J. Appl. Crystallogr* 20 (1987) 139.
- [22] O. Jepsen, A. Burkhardt, O.K. Andersen, *The TB-LMTO-ASAP Program*, Version 4.7, Max-Planck-Institut für Festkörperforschung, Stuttgart, Germany, 1999.
- [23] O.K. Andersen, O. Jepsen, *Phys. Rev. Lett.* 53 (1984) 2571.
- [24] W.R.L. Lambrecht, O.K. Andersen, *Phys. Rev. B: Condens. Matter* 34 (1986) 2439.
- [25] P.E. Blöchl, O. Jepsen, O.K. Andersen, *Phys. Rev. B: Condens. Matter* 49 (1994) 16223.
- [26] R. Dronskowski, P.E. Blöchl, *J. Phys. Chem.* 97 (1993) 8617.
- [27] S.-Q. Xia, S. Bobev, *Inorg. Chem.* 45 (2006) 7126.
- [28] W. Dörrscheidt, G. Savelsberg, J. Stöhr, H. Schäfer, *J. Less-Common Met* 83 (1982) 269.
- [29] N. May, H. Schäfer, *Z. Naturforsch* 29 (1974) 20.
- [30] V. Hlukhyy, S. Eck, T.F. Fässler, *Inorg. Chem.* 45 (2006) 7408.
- [31] E. Parthé, B. Chabot, in: K.A. Gscheidner Jr., L. Eyring (Eds.), *Handbook of the Physics and Chemistry of Rare Earths*, vol. 6, Elsevier Science, Amsterdam, 1984.
- [32] P. Rogl, in: K.A. Gscheidner Jr., L. Eyring (Eds.), *Handbook of the Physics and Chemistry of Rare Earths*, vol. 7, Elsevier Science, Amsterdam, 1984.
- [33] D.M. Proserpio, G. Chacon, C. Zheng, *Chem. Mater.* 10 (1998) 1286.

- [34] L. Pauling, *The Nature of the Chemical Bond*, Cornell University Press, Ithaca, NY, 1960.
- [35] G.A. Papoian, R. Hoffmann, *Angew. Chem. Int. Ed.* 39 (2000) 2408.
- [36] C. Lupu, J.-G. Mao, J. Rabalais, A.M. Guloy, *Inorg. Chem.* 42 (2003) 3765.
- [37] W. Müller, *Z. Naturforsch* 29 (1974) 304.
- [38] D.A. Hansen, L.J. Chang, *Acta Crystallogr. B* 25 (1969) 2392.
- [39] M.A. Zhuravleva, D. Bilc, R.J. Pcionek, S.D. Mahanti, M.G. Kanatzidis, *Inorg. Chem.* 44 (2005) 2177.
- [40] E.J. Gabe, Y. le Page, P.-P. Charland, F.L. Lee, P.S. White, *J. Appl. Cryst.* 22 (1989) 384.
- [41] I.R. Harris, G.V. Raynor., *J. Less-Common Met.* 9 (1965) 7.
- [42] R.E. Schaak, T.E. Mallouk, *Chem. Mater.* 14 (2002) 1455.
- [43] S. Cirafici, A. Palenzona, P. Manfrinetti, *J. Less-Common Met* 90 (1983) 49.
- [44] R.D. Shannon, C.T. Prewitt, *Acta Crystallogr B* 25 (1969) 925. (B26 (1970) 1046).
- [45] C. Kittel, *Introduction to Solid State Physics*, seventh ed., John Wiley and Sons, Hoboken, NJ, 1996.